1   *Electronic supplementary information*

2   Graphene oxide/ graphitic carbon nitride/ polyamide oxime nanofibers

3   with adsorption and photocatalytic reduction of uranium from seawater

4   *Shiliang Qin[a], Jianang Sha[b,c] Peipei Yang[a,b]*, Songwei Li[a]*, Chuntai Liu[a], Changyu Shen[a]*

5   [a] State Key Laboratory of Structural Analysis, Optimization and CAE Software for

6   Industrial Equipment, National Engineering Research Center for Advanced Polymer

7   Processing Technology, Key Laboratory of Materials Processing and Mold (Ministry of

8   Education), Zhengzhou University, Zhengzhou 450002, China.

9   [b] Xiamen Branch of Luoyang Ship Material Research Institute, Xiamen, Fujian 361116,

10   China.

11   [c] National Key Laboratory of Marine Corrosion and Protection, Xiamen, Fujian 361116,

12   China.

13   [*] Corresponding author. E-mail address: lisw@zzu.edu.cn; peipeiyang@zzu.edu.cn

14

1. Supporting experimental Section

1.1 Characterization

The FT-IR spectra of the samples were obtained by transmission test on a Nicolet 6700 FT-IR spectrometer. The operating conditions of the instrument were as follows: 32 scans with a scanning range of 4000-500 cm^{-1}. X-ray photoelectron spectroscopy was characterized by Thermo Scientific K-alpha X-ray photoelectron spectrometer. During the test, the operating voltage was 12 kV, the filament current was 6 mA, the full-spectrum scanning pass energy was 150 eV, and the narrow-spectrum scanning pass energy was 50 eV. The pressure in the analysis chamber was $10^{-8} \sim 10^{-7}$ Pa. The microstructure of the nanofibers was observed by ZEISS Gemini 300 scanning electron microscope. The samples were treated with 10 mA gold injection to enhance the electrical conductivity. The operating voltage was 10 kV during the test. UV-visible diffuse reflectance spectroscopy was performed using Shimadzu UV 3600I Plus UV-visible near-infrared spectrophotometer with a slit width of 2.0, the test range was 200-600 nm, and the data interval was 1 nm. The photocurrent response, electrochemical impedance spectroscopy (EIS) was performed on a three-electrode CHI660e electrochemical workstation at Shanghai Chenhua Instrument Co., Ltd. The three-electrode system consists of platinum plate electrode, Ag/AgCl reference electrode and FTO working electrode. The electrolyte was 0.5 mol L^{-1} Na$_2$SO$_4$ solution. The photocurrent response test uses a 300W lamp as the light source with a bias of 0.6 V. During EIS test, the frequency range is 0.01 Hz-100 kHz, and the signal amplitude is 10 mV.

The Bruker820-MS inductively weighted plasma mass spectrometer from Bruker, a German company, can be used for qualitative and quantitative analysis of trace metal

38 element concentrations in seawater. The test range is l μg L^{-1}-500 μg L^{-1}. PerkinElmer

39 Optima-7000 DV in the United States inductively coupled plasma atomic emission

40 spectrum can be used to dissolve Liquid of high concentration of metal elements content

41 in qualitative and quantitative analysis, the test scope for 1 mg L^{-1}-500 mg L^{-1} (higher than

42 500 mg L^{-1} concentration of diluted to determine accurate). Fluorescence spectra (PL) and

43 time-resolved spectra (TR-PL) were measured using the Edinburgh FLS980 steady-

44 state/transient fluorescence spectrometer.

45 1.2 Preparation of the GO

46 5 g graphite power and 115 mL H_2SO_4 were stirred for 1 h in the ice bath. 30 g $KMnO_4$

47 was slowly put into the above solution and reacted at 0-3 °C for 3 h. Then, the solution was

48 heated to 50 °C and stirred for 45 min. 400 mL of H_2O was added and stirred for 15 min

49 while the temperature was remained at 50 ± 5 °C. 300 mL of H_2O and 360 g, 5% of H_2O_2

50 were added and the solution was stirred for 15min. Finally, wash the solution with

51 deionized water to a neutral pH.

52 1.3 Preparation of the g-C$_3$N$_4$

53   10 g of urea was placed in a ceramic crucible and heated in a tube furnace at 550 °C

54 for 3 h at a rate of 5 °C min^{-1}. The rate of cooling after the reaction is also 5 °C min^{-1}. When

55 sample reaches room temperature, the g-C$_3$N$_4$ was acquired. At last, place the g-C$_3$N$_4$ into

56 a mortar and slowly grind them to a powder, for further use.

57 1.4 Electrospinning parameter

58   **PAO porous nanofiber film:** The spinning parameters were set as follows: positive

59 voltage 15 kV, negative voltage -3 kV. the speed of the receiver was set at 100 r min^{-1}, the

60 emission speed of the spinning nozzle was 0.06 mm min^{-1}, the distance between the needle

61 and the receiver was 15 cm, the translation distance was 10 mm, the spinning time was set

62 at 8 h, and the spinning temperature was 25 °C.

63 **GO/g-C$_3$N$_4$/PAO porous nanofiber film:** The spinning parameters were set: the

64 positive voltage was 18 kV and the negative voltage was -3 kV. the receiver speed was 100

65 r min^{-1}, the translation distance was 10 mm, and the needle distance from the receiver was

66 15 cm. the emission speed of the spinning nozzle was 0.06 mm min^{-1}, the spinning time

67 was set to 8 h, and the spinning temperature was 25 °C.

68 **1.5 Uranium adsorption assay**

69 0.01 g adsorbent was added to a beaker containing 500 mL and 100 mg L^{-1} uranyl ion

70 solution. The pH of uranyl ion solution was adjusted with 0.1 mol L^{-1} HNO$_3$ and 0.1 mol

71 L^{-1} NaHCO$_3$. The uranium solution was irradiated with a xenon lamp (1 kW m^{-2}) for

72 adsorption. Meanwhile, the adsorption was also carried out under the condition of dark.

73 After the adsorption, the adsorbed solution was measured and the uranyl ion concentration

74 of the adsorbed solution was determined by Inductively Coupled Plasma-Atomic Emission

75 Spectrometry (ICP-AES). According to the measured experimental data, the formula was

76 adopted:

$$q_e = (C_0 - C_e) * \frac{V}{m}$$

77 (S1)

78 Where q_e (mg g^{-1}) is the adsorption capacity of the adsorbent after adsorption

79 equilibrium; C_0 and C_e (mg L^{-1}) stand for initial and residual concentration of uranium,

80   respectively; V is the volume of the solution (L) and *m* is the mass of the absorbent (g).

1.6 Kinetics studies

In the study of adsorption kinetics, the pseudo-first-order (S2), pseudo-second-order (S3) models and Elovich (S4) models were employed to interpret the mechanism controlling the adsorption process. The nonlinear form of the two models were expressed by the following Eqs.

S2-S4:

$$q_t = (1 - Ae^{(-k_1 * t)})$$ (S2)

$$q_t = (t * k_2 * q_e^2)/(1 + k_2 * q_e * t)$$ (S3)

$$q_t = \frac{1}{\beta} ln(\alpha\beta t)$$ (S4)

Where q_t and q_e (mg g^{-1}) stand for the adsorption capacity of U(VI) at time t (min) and at equilibrium, respectively. k_1 (min^{-1}) and k_2 (g (mg^{-1} min)$^{-1}$) are the rate constants, respective. α belongs to the initial absorbance (mg (g*min)$^{-1}$), and β is the desorption constant (g mg^{-1}).

1.7 Isotherms studies

In order to determine the maximum adsorption capacity of adsorbent , the adsorption isotherms were investigated Langmuir model (S6) and Freundlich (S7) models. were used to simulate the adsorption process of adsorbent.

98   S5-S7:

$$q_e = q_m(b * C_e)/(1 + b * C_e) \qquad \text{(S5)}$$

$$q_e = kC_e^{(\frac{1}{n})} \qquad \text{(S6)}$$

$$\ln q_e = \ln q_m - \beta\varepsilon^2 \qquad \text{(S7)}$$

Where C_e (mg L^{-1}) is the residual U(VI) concentration, q_e (mg g^{-1}) stand for the adsorption capacity at equilibrium. k (L mg^{-1}) belongs to Langmuir constant related to the energy of the adsorbent and q_m (mg g^{-1}) represents the saturation adsorption capacity. β is the activity coefficient, ε is the Polanyi potential.

1.8 Competitive adsorption

Uranyl and some coexisting metal ions were dissolved into simulated seawater at 100 times their actual concentration. Then 10 mg of GO/g-C$_3$N$_4$/PAO adsorbent was added to the mixing solution to perform the competitive adsorption assay. After 12 h of adsorption under simulated sunlight irradiation (or dark condition), the solution was filtered and a small amount of clear liquid was taken to test the concentration of remaining metal ions.

1.9 Regeneration experiments

0.01 g of GO/g-C$_3$N$_4$/PAO was added into 200 mL uranyl solution (C_0= 100 mg L^{-1}, pH=6). The concentration of uranyl ion in supernatant was determined by ICP-AES after 3 h of adsorption under light. The adsorbent after uranium adsorption was washed with deionized water. Then, the adsorbent material after uranium adsorption was appended to a

117 20 mL elution solution (0.1 mol L^{-1} NaOH). The concentration of uranyl ions was

118 determined by ICP-AES. Eventually, the elution efficiency of U(VI) ions was calculated.

119 Repeat this experiment operation ten times.

120 **1.10 Real seawater adsorption experiment**

121 1 mg of the adsorbing material was put into a shaped bottle, including 5 L of nature

122 seawater. Then, put the adsorbent into the beaker to irradiate for adsorption under the

123 condition of 300W, 1 kw cm^{-2}. After the adsorption, the solution was transferred to the

124 centrifuge tube for centrifugation and then the supernatant was extracted and the

125 concentration of residual uranium ion was detected by ICP-MS.

126 **2 Supporting figs and tables**
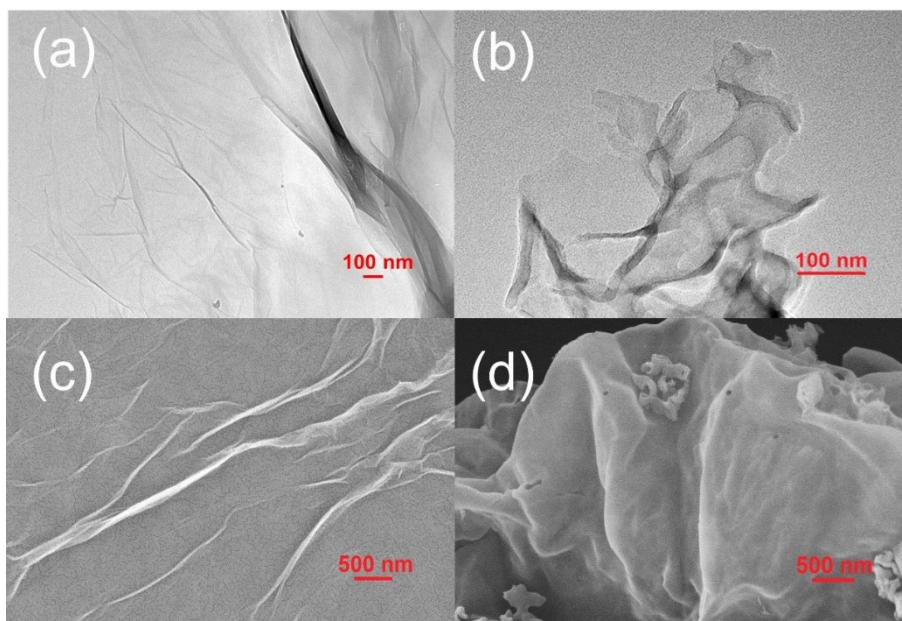
127

128 **Fig. S1** TEM images of (a) GO and (b) g-C$_3$N$_4$; SEM images of (c) GO and (d) g-C$_3$N$_4$.
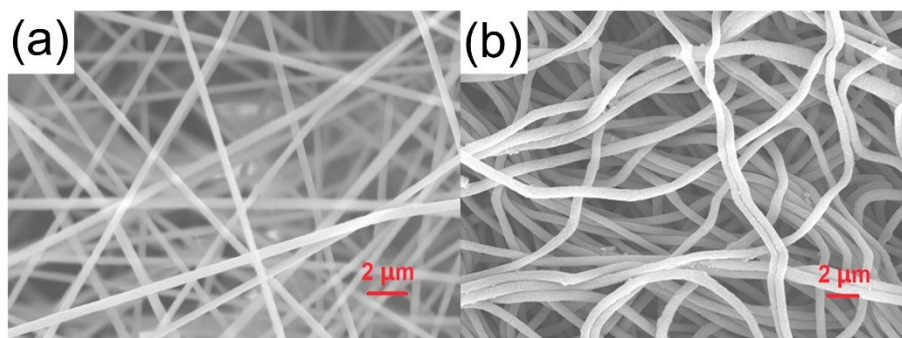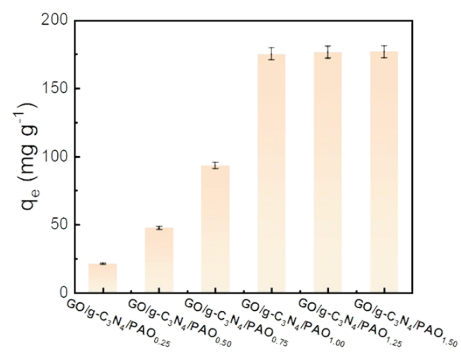
129

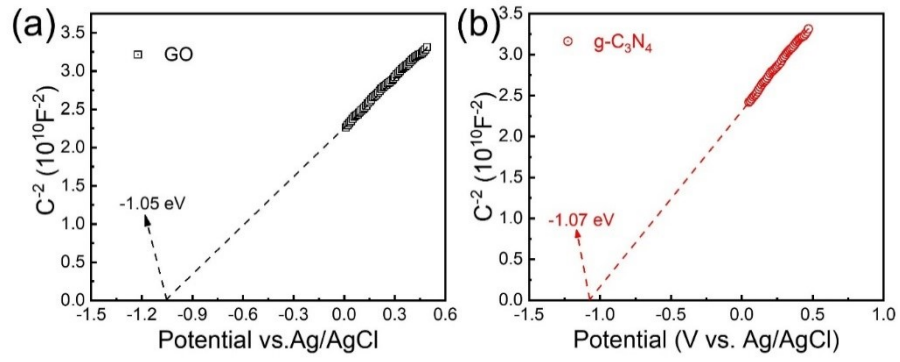130 **Fig. S2** SEM images of (a) PAN nanofiber and (b)PAO nanofiber.
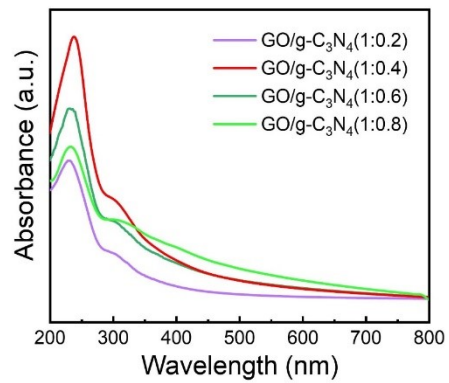
131

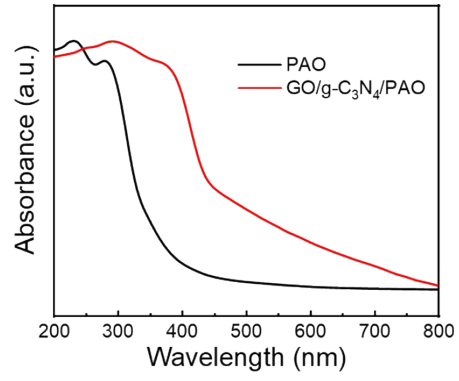132 **Fig. S3** UV-vis DRS spectra of GO and g-C$_3$N$_4$ with different ratios.

133

134 **Fig. S4** The adsorption capacity of GO/g-C$_3$N$_4$ and PAN amidoxime in different
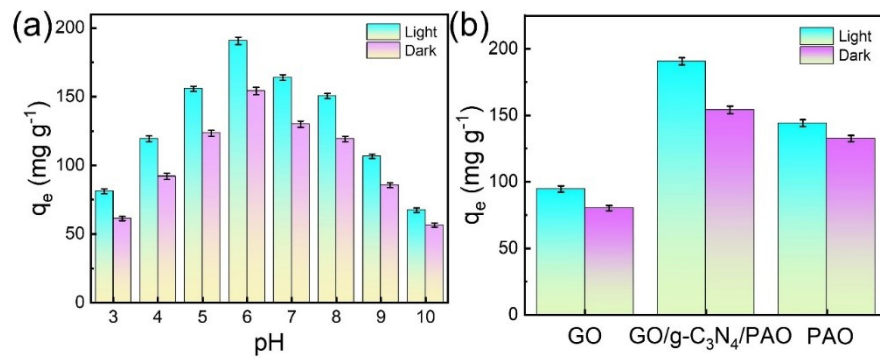
135 proportions.

136

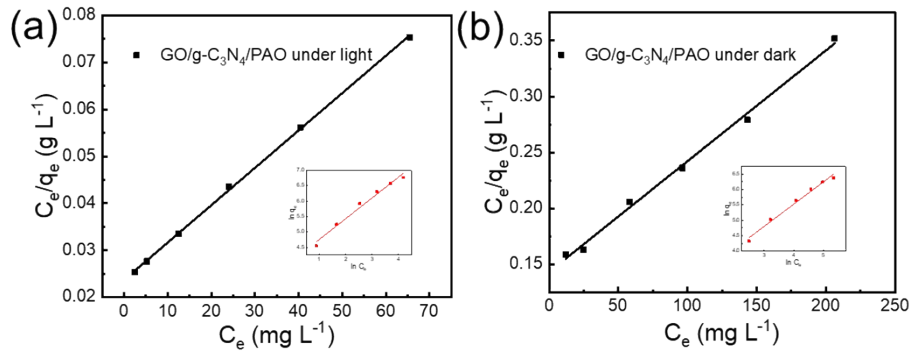137 **Fig. S5** Mott-Schottky plots of (a) GO and (b) g-C_3N_4.

138
139   **Fig. S6** UV-vis DRS spectra of GO/g-C$_3$N$_4$/PAO, PAO.

140

Fig. S7 (a) Effect of pH on the light-dark adsorption profile of GO/g-C$_3$N$_4$/PAO (C$_0$=99.9 mg L^{-1}, m/v = 0.5 g L^{-1}); (b) The effect on the adsorption of GO, PAO and GO/g-C$_3$N$_4$/PAO under both light and dark conditions.
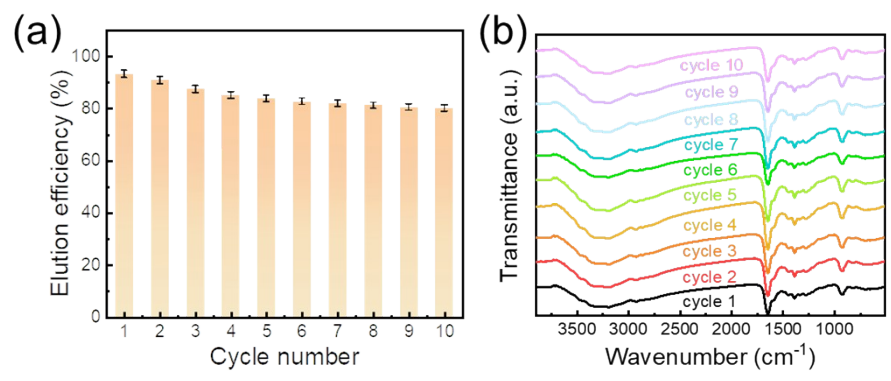
144

Fig. S8 Fitting curves of GO/g-C$_3$N$_4$/PAO adsorbent to langmuir and freundlich models (inset) under (a) simulated daylight and (b) dark conditions (pH = 6, t = 300 min, m/v = 0.5 g L^{-1}).
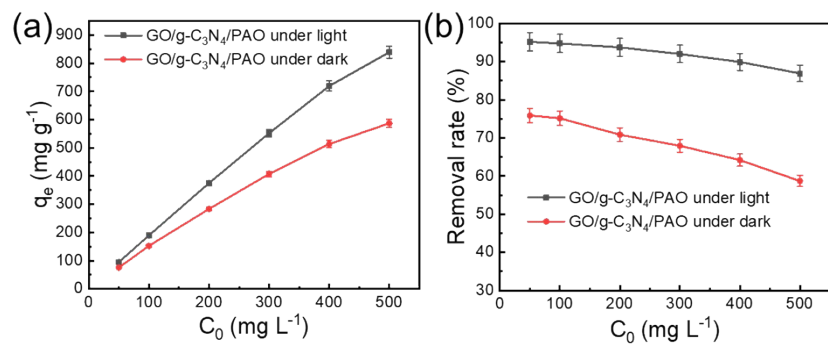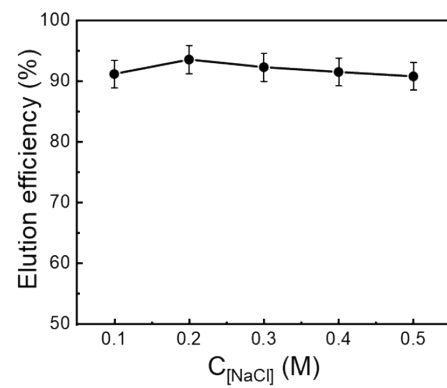
148

149 **Fig. S9** (a) Effects of different uranyl concentrations on GO/g-C$_3$N$_4$/PAO adsorption

150 capacity under light and dark conditions. (b) Removal rates at different uranyl
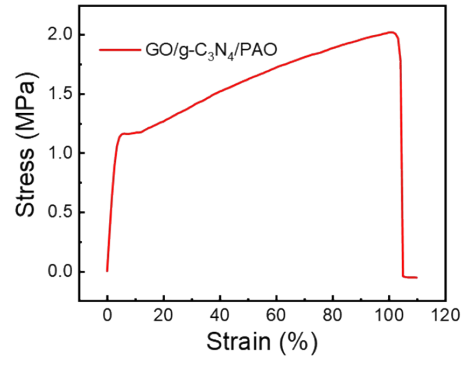
151 concentrations.

152 .

153

Fig. S10 (a) Experiments on the renewable cycle of GO/g-C$_3$N$_4$/PAO. (b) FT-IR of

GO/g-C$_3$N$_4$/PAO after ten cycles after ten cycles.
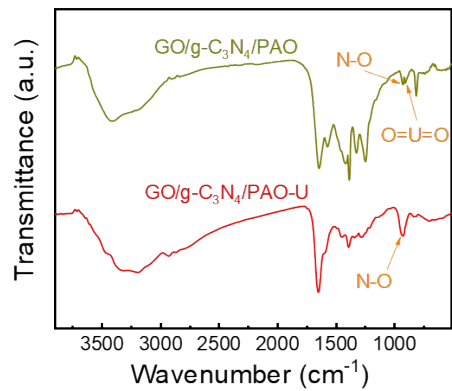
156

157 **Fig. S11** Effect of salt ion strength on adsorption properties of materials.

158

159 **Fig. S12** The stress-strain curve of GO/g-C$_3$N$_4$/PAO.

160

161 **Fig. S13** FT-IR spectra of GO/g-C$_3$N$_4$/PAO before and after uranium adsorption.
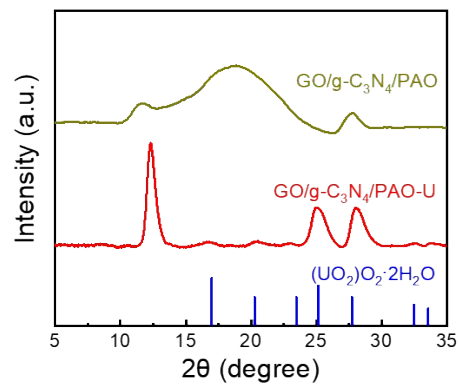
162

163 **Fig. S14** XRD before and after uranium adsorption by GO/g-C$_3$N$_4$/PAO.

164

165 **Fig. S15** (a) High-resolution spectra of C 1s of GO/g-C$_3$N$_4$/PAO before adsorption of

166 uranyl ions; (b) High-resolution spectra of C 1s of GO/g-C$_3$N$_4$/PAO after adsorption of

167 uranyl ions.

168

Table S1 Kinetic parameters of adsorption of uranyl ions

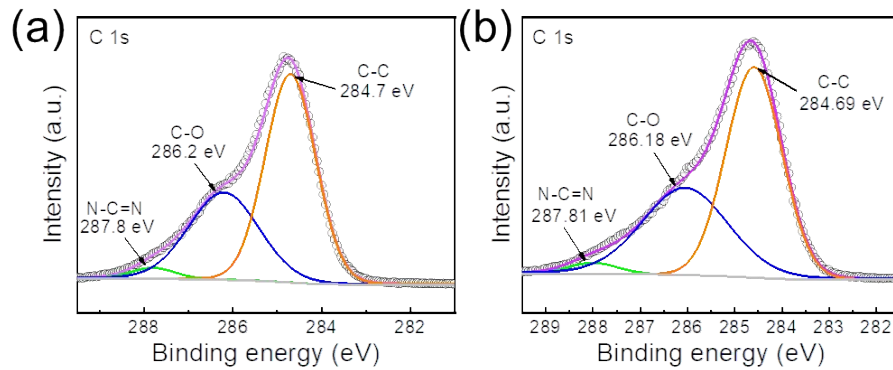| Adsorbents	Pseudo-second-order			Pseudo-first-order		
	$q_{e2, exp}$ (mg g^{-1})	R^2	k_2 (g mg^{-1} min^{-1})	q_{e1}^{cal} (mg g^{-1})	R^2	k_1 (min^{-1})
GO/g-C$_3$N$_4$/PAO -light	196.08	0.9995	7.79*10^{-4}	89.57	0.9181	0.0185
GO/g-C$_3$N$_4$/PAO -dark	156.25	0.9996	10.60*10^{-4}	67.35	0.9271	0.0166

169

170

Table. S2 Thermodynamic parameters of adsorbed uranyl

Adsorbents	Langmuir isotherm			Freundlich isotherm		
	q_m (mg g^{-1})	b (L mg^{-1})	R^2	K (L mg^{-1})	n	R^2
GO/g-C$_3$N$_4$/PAO -light	1256	0.039	0.9993	59.15	1.49	0.979
GO/g-C$_3$N$_4$/PAO -dark	1010	0.007	0.9945	13.89	1.37	0.984

171

172

Table S3 The elution efficiency of different desorption agents

Eluent	Elution efficiency (%)
NaOH	93.3
NaHCO$_3$	60.3
HCl	46.6
H$_2$O	6.3
Na$_2$CO$_3$	61.9

173

174 **Table S4** Uranium sorption performance of various adsorbing materials

Adsorbents	q_e (mg g^{-1})	T (day)	Reference
Fe$_3$O$_4$@TiO$_2$-AO	0.0875	33	[1]
Ti$_3$C$_2$-AO-PA	4.94	/	[2]
MP-PAO	5.80	24	[3]
CI-PAO	6.17	28	[4]
PAN/ZIF-67	2.03	36	[5]
PAGM-1	6.21	30	[6]
GO/g-C$_3$N$_4$/PAO	10.39	30	This work

175

176 **Reference**

177 1.   N. Li, P. Gao, H. Chen, F. Li and Z. Wang, Amidoxime modified Fe_3O_4@TiO_2

178   particles for antibacterial and efficient uranium extraction from seawater,

179   *Chemosphere*, 2022, **287**,132137.

180 2.   D. Zhang, L. Liu, B. Zhao, X. Wang, H. Pang and S. Yu, Highly efficient extraction

181   of uranium from seawater by polyamide and amidoxime co-functionalized MXene,

182   *Environ. Pollut*, 2023, **317**,120826.

183 3.   H. Wang, B. Zheng, T. Xu, M. Cao, F. Gao, G. Zhou, C. Ma, J. Dang, W. Yao, K.

184   Wu, T. Liu, Y. Yuan, Q. Fu and N. Wang, Macroporous hydrogel membrane by

185   cooperative reaming for highly efficient uranium extraction from seawater, *Sep.

186   Purif. Technol.*, 2022, **289**,120823.

187 4.   H. Wang, T. Xu, B. Zheng, M. Cao, F. Gao, G. Zhou, C. Ma, J. Dang, W. Yao, K.

188   Wu, T. Liu, Y. Yuan, Q. Fu and N. Wang, Cuttlefish ink loaded polyamidoxime

189   adsorbent with excellent photothermal conversion and antibacterial activity for

190   highly efficient uranium capture from natural seawater, *J. Hazard. Mater*, 2022,

191   **433**,128789.

192 5.   W. Li, Y.-Y. Liu, Y. Bai, J. Wang and H. Pang, Anchoring ZIF-67 particles on

193   amidoximerized polyacrylonitrile fibers for radionuclide sequestration in

194   wastewater and seawater, *J. Hazard. Mater*, 2020, **395**,122692.

195 6.   H. Li, J. Sun, S. Qin, Y. Song, Z. Liu, P. Yang, S. Li, C. Liu and C. Shen, Zwitterion

196   Functionalized Graphene Oxide/Polyacrylamide/Polyacrylic Acid Hydrogels with

197   Photothermal Conversion and Antibacterial Properties for Highly Efficient

198   Uranium Extraction from Seawater, *Adv. Funct. Mater*, 2023, **33**,2301773.

199